Cerebral Cortex, 2017; 1–13

doi: 10.1093/cercor/bhx233
Original Article

ORIGINAL ARTICLE

Random Recurrent Networks Near Criticality Capture the Broadband Power Distribution of Human ECoG Dynamics

Rishidev Chaudhuri[1,2], Biyu J. He[3,4] and Xiao-Jing Wang[2,5]

[1]Center for Learning and Memory and Department of Neuroscience, The University of Texas at Austin, Austin, TX 78712, USA, [2]Center for Neural Science, New York University, New York, NY 10003, USA, [3]National Institute of Neurological Disorders and Stroke, National Institutes of Health, Bethesda, MD 20892, USA, [4]Departments of Neurology, Neuroscience and Physiology, and Radiology, Neuroscience Institute, New York University Langone Medical Center, New York, NY 10016, USA and [5]NYU-ECNU Joint Institute of Brain and Cognitive Science, NYU Shanghai, Shanghai 200122, China

Address correspondence to Xiao-Jing Wang, Center for Neural Science, New York University, 4 Washington Place, New York, NY 10003, USA. Email: xjwang@nyu.edu

Abstract

Brain electric field potentials are dominated by an arrhythmic broadband signal, but the underlying mechanism is poorly understood. Here we propose that broadband power spectra characterize recurrent neural networks of nodes (neurons or clusters of neurons), endowed with an effective balance between excitation and inhibition tuned to keep the network on the edge of dynamical instability. These networks show a fast mode reflecting local dynamics and a slow mode emerging from distributed recurrent connections. Together, the 2 modes produce power spectra similar to those observed in human intracranial EEG (i.e., electrocorticography, ECoG) recordings. Moreover, such networks convert spatial input correlations across nodes into temporal autocorrelation of network activity. Consequently, increased independence between nodes reduces low-frequency power, which may explain changes observed during behavioral tasks. Lastly, varying network coupling causes activity changes that resemble those observed in human ECoG across different arousal states. The model links macroscopic features of empirical ECoG power to a parsimonious underlying network structure, and suggests mechanisms for changes observed across behavioral and arousal states. This work provides a computational framework to generate and test hypotheses about cellular and network mechanisms underlying whole brain electrical dynamics, their variations across states, and potential alterations in brain diseases.

Key words: dynamics, electrocorticography, neural networks, power spectrum, bifurcation

Introduction

The power spectrum of electric field potentials recorded from the brain consists of oscillatory peaks, indicative of underlying rhythmicity, riding on top of a broadband "$1/f^{\beta}$" slope (power falls off with frequency, following $P \approx A/f^{\beta}$, where β is the power-law exponent), which constitutes the majority of signal power (Freeman and Zhai 2009; Onton and Makeig 2009; Miller et al. 2009a; He et al. 2010; Ray and Maunsell 2011; Manning et al. 2012). Research over the past decades has significantly advanced our understanding of the functional roles and

generative mechanisms of brain oscillations at different frequencies (Buzsáki 2006; Fries 2009; Wang 2010; Jensen et al. 2012; Womelsdorf et al. 2014). However, the origins of the arrhythmic signal contributing the $1/f^{\beta}$ component of the spectrum remain elusive (Bedard and Destexhe 2009; Roberts et al. 2015).

Recent research has shown that this arrhythmic, broadband field potential cannot be explained as summation of many oscillations (Miller et al. 2009b; He et al. 2010). By contrast, it appears to be a distinct type of brain activity, potentially a macroscopic manifestation of the irregular firing of cortical neurons (Miller et al. 2009a; He 2014). In particular, broadband power in the gamma-frequency (>30 Hz) range correlates with population firing rate (Manning et al. 2009; Whittingstall and Logothetis 2009; Ray and Maunsell 2011; Buzsáki and Wang 2012) and exhibits functional specificity across a variety of tasks (Crone et al. 1998; Miller et al. 2009b; Ossandón et al. 2011; Bouchard et al. 2013). In the very low-frequency range (<1 Hz), the slope of the power spectrum (i.e., the power-law exponent β)—an index of the amount of long-time autocorrelation in the signal—is reduced during a visual detection task (He et al. 2010). Despite these results demonstrating the functional significance of arrhythmic, broadband activity, a mechanistic account explaining the full frequency range of its signature power spectrum remains lacking.

Multiple studies using local field potential (LFP) and ECoG recordings have found that for frequencies greater than about 1 Hz, the power law exponent β is typically between 2 and 3 (Freeman and Zhai 2009; Manning et al. 2009; Milstein et al. 2009; Miller et al. 2009a; He et al. 2010) (though also see Bedard et al. 2006, which finds slopes of −1 and −3 at low and high frequencies, respectively). A study using DC-recording revealed the shape of human ECoG power spectra across a wide range of frequencies, from 0.01 to >100 Hz (He et al. 2010). The power spectra exhibit a distinctive shape: at very low frequencies (<0.1 Hz) and above 1 Hz, power scales approximately proportional to the inverse-square of frequency ($P \sim 1/f^2$), while power spectra in the intermediate frequency range (0.1–1 Hz) are much flatter. This tripartite shape was conserved across subjects, albeit with differences in the locations of the transitions between the decaying and flat regions of the spectrum.

Here, we use a network model to investigate the potential neural-circuit-level origins of the broadband signal in field potential recordings. We find that the power spectrum is well fit as the combination of 2 linear modes, which sum to produce the characteristic tripartite shape of the empirically observed human ECoG spectrum. We then show that such a power spectrum generically emerges from the activity of a recurrent network model with nodes randomly connected to each other, provided that the net excitation (i.e., excess of excitation over inhibition) between nodes roughly balances the intrinsic decay of activity. Thus, the network is near a bifurcation point and in this sense is close to dynamical criticality (Chialvo 2010; Beggs and Timme 2012; Deco and Jirsa 2012; Palva et al. 2013; Priesemann et al. 2014; Bellay et al. 2015; Roberts et al. 2015). We characterize the dependence of the power spectrum on network parameters and on input structure, and show that such random recurrent networks naturally convert correlations across neurons in the input into temporal correlations in network activity. We then extend the architecture and investigate networks with a distance-dependent connectivity profile and networks where the nodes are themselves clusters of sub-nodes. Our analyses link empirically observed human ECoG power spectra to plausible underlying neural network dynamics and suggest potential circuit-level explanations for changes in the low-frequency power spectrum across behavioral and arousal states.

Materials and Methods

Empirical Human ECoG Data

All empirical data have been previously reported in He et al. (2010) and further details are in SI, Section 1. Briefly, the study included 8 patients undergoing surgical treatment for intractable epilepsy. In Patients #1–#5, artifact-free, interictal-spike-free ECoG data were collected from both wakefulness and slow-wave sleep (SWS, sleep stages 3/4). Awake, REM and SWS were determined by standard sleep stage scoring based on the conjunction of ECoG and video recordings. In Patient 4, REM sleep was recorded and identified based on active eye movements in the video record and the electrooculogram (EOG). SWS identification primarily used ECoG delta power. The high-frequency cutoffs of the power spectra are set by an anti-aliasing filter, and this cutoff differs between patients. The recordings use a Neuroscan Synamps^2 RT amplifier. The noise spectrum of the amplifier is reported in Figure S6 of He et al. (2010); this noise spectrum is not flat but, in the range we consider, is 2 orders of magnitude less than the signal, and the noise spectrum is additive with the brain signal so is negligible. We also note that the amplifier is a DC amplifier and that the amplification response is flat in the frequency range of physiological signals.

Lorentzian Fit to the Data

We fit the empirical power spectra with a function of the form (see SI, Section 3 for details):

$$P(f) = C_1\left(\frac{C_2}{f^2} + \frac{1}{f^2 + f_{\text{fast}}^2}\right).$$

Note that, except for a small region of the power spectrum, this function is dominated by the larger of the 2 terms. This is shown in Figure 1C, where the sum of the 2 terms is well-approximated by the maximum. We fit this functional form by minimizing the mean squared difference between the log of the empirical and predicted power spectra using the fmincon function with an interior-point solver in Matlab 9.0.0 (Mathworks Inc, Natick, MA). For all figures except Figure 8, we fit to the region below 5 Hz. For Figure 8 we fit a function that includes a second timescale (see SI, Section 12), and fit up to 50 Hz.

We test for spatial structure in the fitted frequencies (f_{fast}) in 2 ways. First, we calculate the correlation between the frequencies of neighboring electrodes. Second, we linearly regress the fitted frequencies for each electrode onto the electrode position (i.e., x and y position in the electrode array) to look for a linear gradient. In both cases we generate a null distribution by repeatedly shuffling the assignment of frequencies to electrodes and recomputing the correlations between neighbors and the regression onto electrode position. We then compare the unshuffled correlation and r^2 values to those from the shuffled frequencies to generate P-values.

Random Network Model

The assumptions underlying the network model are discussed in SI, Sections 4 and 6. Briefly, we consider a population of nodes (which may be neurons or clusters of neurons) with linear f–I curves. We then assume that the ECoG signal is dominated by the summed recurrent synaptic current into a fraction of neurons in the network (along with the corresponding passive return current). This yields Eqs. (1–3) in the main text. For the simulations in Figure 3, we set $N = 440$, $\tau = 195$ ms, $\gamma = 0.1$ Hz/pA, $\mu_{\text{conn}} = 49.881$ pA/Hz, $\sigma_{\text{conn}} = 4.988$ pA/Hz, $p = 0.2$, and $\alpha = 1/44$

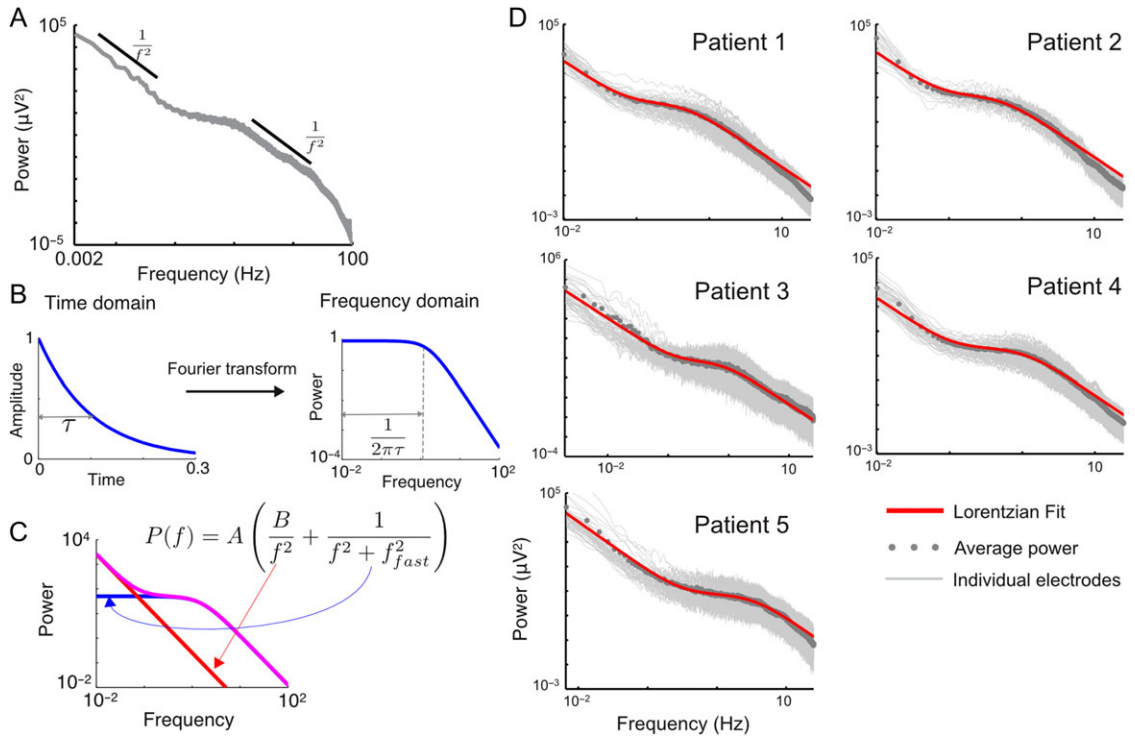

Figure 1. The low-frequency power spectra of human ECoG are well-fit by the sum of 2 Lorentzian functions. (*A*) Average power spectrum from 1 patient in the study of He et al. (2010). The power spectrum resembles a power law with frequency dependence $1/f^2$ at low and high frequencies, with a roughly flat intermediate region. (*B*) The power spectrum of an exponential is a Lorentzian function, which is near-flat at low-frequencies and shows $1/f^2$ scaling at high frequencies, with a transition point set by the time-constant of the exponential. (*C*) The sum of 2 Lorentzian functions yields a shape resembling the power spectrum of Figure 1A, with the "knee" frequency set by f_{fast}. (*D*) Each plot is the power spectrum from 1 patient in He et al. (2010). The light grey traces correspond to recordings from each electrode while the dark grey circles are the averages across all electrodes. Red traces are fits of a sum of 2 Lorentzian functions (corresponding to the functional form shown in Fig. 1C). The functional form is fit to the frequencies below 5 Hz and the data is shown up to 25 Hz. The slope of the power spectrum is steeper for frequencies beyond 25 Hz; see Discussion and Figure 8 for fits to the remainder of the spectrum.

(so that we average over clusters of 10 nodes). Here τ is determined by fitting the network knee frequency. N is arbitrary, and α is chosen to match the ratio of the 2 terms in the Lorentzian fit. μ_{conn} and p are required to satisfy $\gamma p \mu_{conn} \approx 1$, and thus either can be varied provided the other is changed to keep this relationship fixed. σ_{conn} yields the spread of eigenvalues in the cloud of Figure 3C, and provides a corresponding spread of timescales around τ. This variation gets partially averaged away in the equation for the ECoG signal (Eq. 3), and multiple parameter values yield good fits to the empirical data.

Further details on the clustered network and the network with distance-dependent connectivity are in SI, Sections 10 and 11.

Results

Two Modes in the Low-Frequency Power Spectrum

The power-law exponents seen in ECoG power spectra (Fig. 1A) are characteristic of linear systems, which have an autocorrelation function composed of a weighted sum of exponentials. The power spectrum of an exponential function, $e^{-\lambda t}$, is proportional to $\frac{1}{f^2+f_0^2}$, where f is the frequency and $f_0 = \lambda/2\pi$. As shown in Figure 1B, when plotted on a log-log scale these functions (often called Lorentzians) are approximately flat at low frequencies and scale with slope −2 at high frequencies; the transition between the 2 regimes happens at the frequency f_0, which we refer to as the "knee" frequency. Motivated by this observation, we fit the power spectrum from the 5 subjects of He et al. (2010) as the weighted sum of a fast and a slow linear mode (Fig. 1C). The corresponding functional form is as follows:

$$P(f) = C_1\left(\frac{C_2}{f^2+f_{\text{slow}}^2} + \frac{1}{f^2+f_{\text{fast}}^2}\right) \approx C_1\left(\frac{C_2}{f^2} + \frac{1}{f^2+f_{\text{fast}}^2}\right).$$

In the second equation we assume that f_{slow} is small enough to be outside the observational range and can be neglected. Thus, the fit has a single knee frequency, located at f_{fast}.

In Figure 1D we show this fit for the average power spectrum of each of the 5 subjects in the study of He et al. (2010). The functional form accounts for the shape of the power spectrum across several orders of magnitude (with deviations at high frequencies; see Fig. 8). The location of the transition from the initial $1/f^2$ behavior to the flat region is set by the relative contributions of the 2 Lorentzians and hence is determined by the parameter C_2. As previously mentioned, the second transition to $1/f^2$ has location set by f_{fast}. For the 5 patients shown in Figure 1C, the knee frequency (f_{fast}) is at 0.49, 0.55, 0.81, 1.10, and 3.47 Hz, respectively.

In Figure 2, we show the knee frequency (f_{fast}) for individual fits to each electrode in each patient. There is considerable variation in the characteristic frequency across electrodes, with the fastest frequency being 2–5 times the slowest one. However, neighboring electrodes show similar values for the knee frequency, with correlations of 0.35, 0.31, 0.28, 0.32, and 0.33, respectively ($P < 0.002$ for all patients; see Materials and Methods for further details). Moreover, 4 of the 5 subjects (#1,

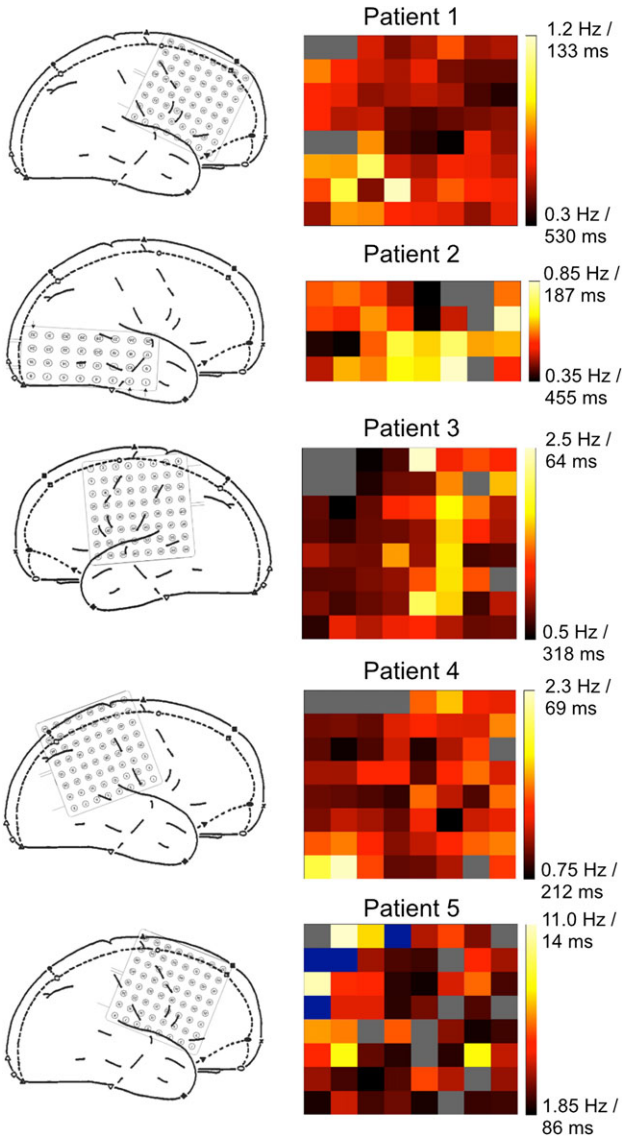

Figure 2. The knee frequency (f_{fast}) for individual electrodes across patients. *Left panel*: Locations of electrodes for each of the 5 patients. *Right panel*: knee frequency for individual electrodes, with location in the heat map corresponding to the electrode locations shown on the left. Electrodes excluded in the study of He et al. (2010) are shown in grey and, for Patient 5, electrodes poorly fit as a sum of Lorentzians are shown in blue. Timescales shown are the time-constants of a linear system with corresponding knee frequency (i.e., $\tau = 1/2\pi f_{knee}$).

#2, #3, and #5) show evidence of a linear gradient in the fitted frequencies, with $r^2 = 0.2871$, 0.2318, 0.1684, and 0.2988, respectively (corresponding P-values of $<10^{-4}$, 0.035, 0.004, and $<10^{-4}$). This suggests that the variation is not random and contains spatial structure (see Discussion).

A Random Network Model for the Power Spectrum

We next construct a recurrent network model which reproduces the observed power spectrum. The model network has N nodes, which could be neurons or networks of neurons. The jth node has activity r_j, which evolves in time according to the following equation:

$$\tau \frac{d}{dt} r_j(t) = -r_j(t) + \gamma \left[\sum_{k=1}^{N} W_{jk} r_k(t) + I_j^{ext}(t) \right]_+ \quad (1)$$

Each node receives input from other nodes in the network (r_k) with weight W_{jk}, along with external input I_j^{ext}, corresponding to input that does not come from within the network. $[\cdot]_+$ is a threshold linearity (i.e., $[x]_+ = \max(x,0)$) and γ is the slope of the firing rate-current curve.

In the absence of input, the firing rate of the jth node decays exponentially to 0 with time-constant τ. This time-constant is taken to be the same across nodes, for convenience, but relaxing this assumption yields near-identical results. Grouping the firing rates into a vector and the weights into a matrix, and assuming that input is large enough that the network rarely encounters the threshold, we can rewrite this equation as follows:

$$\frac{d}{dt}\mathbf{r}(t) = -\frac{\mathbf{r}(t)}{\tau} + \frac{\gamma}{\tau} W \mathbf{r}(t) + \frac{\gamma}{\tau} I^{ext}(t) = A\mathbf{r}(t) + \frac{\gamma}{\tau} I^{ext}(t). \quad (2)$$

Here the matrix $A = (-\mathbb{1} + \gamma W)/\tau$, where $\mathbb{1}$ is the identity matrix.

We assume that the observed field potential recording results from summing together the input current to a subset of network nodes. If network connections are sparse and recurrent input dominates, then the field potential is approximately a weighted sum of the activity of a fraction of network nodes (see SI, Section 4). Thus, if $\phi(t)$ is this summed activity, we have

$$\phi(t) \propto \sum_{j=1}^{\alpha N} r_j(t) \quad (3)$$

Here, $0 < \alpha < 1$ is the fraction of the network we are summing over, and we have written the sum over the first αN nodes for convenience. We will refer to $\phi(t)$ as "network activity." While we consider an equally weighted sum of nodes contributing to ϕ, our analysis can easily be extended to a differentially weighted sum or spatial kernel applied to the nodes.

We choose the connections (the entries of matrix W) to be sparse and random: each entry is nonzero with probability p, and nonzero entries are drawn from a normal distribution: $w_{ij} \sim \frac{1}{N} N(\mu_{conn}, \sigma^2_{conn})$. In Figure 3B, we show the power spectrum of network activity. This reproduces the data for appropriately chosen values of τ, μ_{conn}, and α. Note that μ_{conn} must be set to almost balance the intrinsic decay of network activity (which decays with time-constant τ at each node).

The activity of the multidimensional linear system in Eq. 2 can be thought of geometrically: the vector $\mathbf{r}$ lives in an N-dimensional space with each dimension corresponding to the activity at 1 node (i.e., r_j is the activity along the jth node). The system can be solved by changing the coordinate system and rewriting $\mathbf{r}$ in a new coordinate system whose directions are given by the eigenvectors of the matrix A. These eigenvectors form the natural coordinate system in which to see the activity of A: they provide a decomposition of the network activity into a set of characteristic modes, each of which evolves independently in time with its own characteristic timescale. This decouples an N-dimensional problem into a collection of N one-dimensional problems.

The eigenvectors are defined as vectors $\boldsymbol{v_n}$ that satisfy the equation $A\boldsymbol{v}_n = \lambda_n \boldsymbol{v}_n$, where λ_n is a constant, called the eigenvalue corresponding to the eigenvector $\boldsymbol{v_n}$. The characteristic timescale of network activity corresponding to the eigenvector

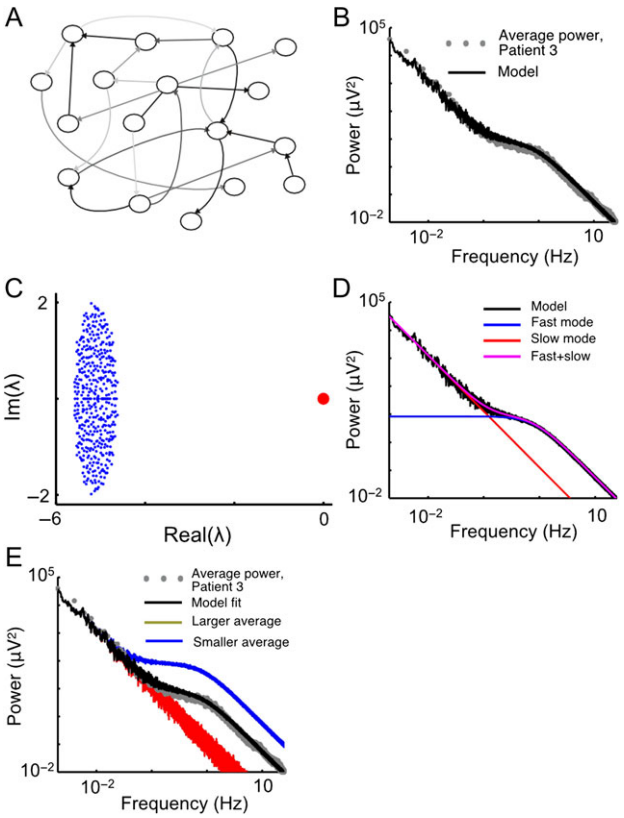

Figure 3. The power spectrum of a random network reproduces observed ECoG power spectra. (*A*) Schematic of a sparse randomly connected network. (*B*) Power spectrum of network activity in a random network where mean connection strengths approximately balance the intrinsic decay of activity. The power spectrum from Patient 3 is shown for comparison. Here $N = 440$, $\tau = 195$ ms, $\gamma = 0.1$ Hz/pA, $\mu_{conn} = 49.881$ pA/Hz, $\sigma_{conn} = 4.988$ pA/Hz, $p = 0.2$, and $\alpha = 1/44$. (*C*) The eigenvalue spectrum of the network coupling matrix shows a cluster of fast modes (in blue) and a single slow mode (in red). (*D*) The power spectrum of the simulated network is the sum (purple) of Lorentzians contributed by the fast modes (blue) and the slow mode (red). (*E*) Effect of spatial averaging on power spectrum. Black: power spectrum from the network in panel (*B*) with the same degree of averaging. Blue: network activity derived by summing over a smaller fraction of the network (here, a single node). Red: network activity derived by summing over a larger fraction of the network (here, all nodes in the network). The slow mode is shared between nodes, while the fast modes are uncorrelated; thus averaging over nodes boosts the contribution of the slow mode. In particular, summing over the entire network yields a power spectrum that shows pure power-law behavior.

υ_n is $-1/\Re\mathrm{e}(\lambda_n)$. Thus, the eigenvalues tell us what timescales the network will show, and the eigenvectors tell us how this activity is distributed across nodes.

To understand how the network model is able to reproduce the data, we consider the distribution of eigenvalues of the network coupling matrix, A. These eigenvalues describe the characteristic temporal modes of the network (see SI for more details). For the randomly connected network we consider, the eigenvalues take a particularly simple form, known from the theory of random matrices (Rajan and Abbott 2006; Ganguli et al. 2008; Tao 2011) and depicted in Figure 3*C*. The network has 1 slow mode, here corresponding to a negative eigenvalue near 0 (the red point in Fig. 3*C*), and $N - 1$ fast modes, which are centered around $-1/\tau$ (the cloud of blue points in Fig. 3*C*). If the external input to each node is independent, then the power spectrum of network activity can be approximately broken up into contributions from each of these 2 sets of modes (Fig. 3*D* and see SI, Sections 7 and 8 for derivation), and is given by the following equation:

$$P(f) \approx K\left(\frac{\alpha}{f^2 + (\lambda_{slow}/2\pi)^2} + \frac{1-\alpha}{f^2 + (\lambda_{fast}/2\pi)^2}\right). \quad (4)$$

If λ_{slow} is small (i.e., the corresponding mode is very slow), the power spectrum is of the same form as the fit in Figure 1, with the relative contribution of slow and fast modes determined by α (the fraction of the network averaged over), and the location of the knee frequency given by $-\lambda_{fast}/2\pi$.

The eigenvalue λ_{slow} emerges from internode recurrent interactions: in response to an input, nodes of the network excite each other, reverberating the signal around the network and slowing its decay. λ_{slow} is approximately located at $(\gamma p \mu_{conn} - 1)/\tau$, and when recurrent excitation balances the intrinsic decay of activity this is very close to 0. In this case signals reverberate in the network for a long time, producing a slowly decaying autocorrelation function.

On the other hand, λ_{fast} is set by the intrinsic properties of each network node and is approximately located at $-1/\tau$. There are $N - 1$ such fast modes, each with time-constant approximately equal to τ. Note that if each node is a cluster of neurons, the time-constant τ itself emerges from underlying recurrent interactions; we return to this issue later.

Since the slow mode emerges from internode interactions, it corresponds to a globally distributed pattern of network activity. This is given by the eigenvector, υ_{slow}, corresponding to the eigenvalue λ_{slow}. υ_{slow} can be thought of as a slowly varying background state of the network that all the nodes are coupled to; in particular, for low variability in connection strengths, υ_{slow} has approximately equal weight at each node. By contrast, the fast modes are uncorrelated with each other and thus different nodes participate in a particular fast mode to greatly varying degrees. As a consequence of this global distribution of the slow mode, the network model accounts for the common observation that low-frequency activity (i.e., slow timescales) shows a wider spatial correlation than activity at high frequencies (von Stein and Sarnthein 2000; Leopold et al. 2003; Buzsáki 2006).

Moreover, because of the global distribution of the slow mode, averaging activity across multiple nodes in a network will emphasize the slow mode and increase its contribution to the observed power spectrum. This can be seen in Eq. (4) above, where the relative contributions of the slow and fast modes are given by α, the fraction of the network averaged over to generate the network activity. In Figure 3*E*, we show the effect of averaging over different fractions of the network. In particular, averaging over a large fraction of nodes yields a power spectrum dominated by the $1/f^2$ term. Note, however, that if there exist multiple recurrent networks, each described by an equation such as Eq. (2) but only weakly coupled to each other, then averaging across nodes belonging to these different networks will not change the shape of the power spectrum, because the weak coupling between these networks would not generate another slow mode.

While the network model has purely excitatory connections between the nodes (recall that these nodes may, in turn, be clusters of neurons), similar results hold for a network with inhibitory connections (Fig. 4*A*). As previously argued (Rajan and Abbott 2006; Ganguli et al. 2008), and as depicted in Figure 4*B*, a randomly connected network where a subset of nodes make inhibitory connections onto their targets has an eigenvalue spectrum that is similar to that of Figure 3. Here the location of the slow network mode depends on the difference

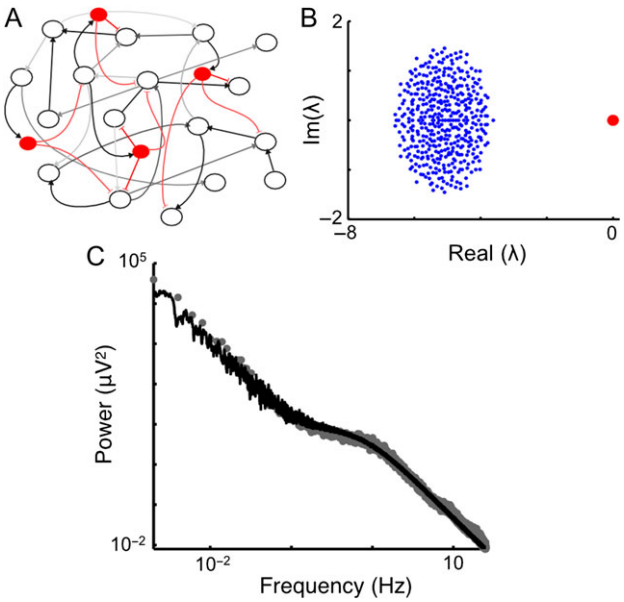

Figure 4. Power spectrum of a random network with both excitatory and inhibitory connections. (*A*) Schematic of network, as in Figure 3*A* but with the incorporation of interneurons shown in red. (*B*) Eigenvalue spectrum of the network. (*C*) Power spectrum of network activity (black) along with data from Patient 3 (grey filled circles).

between excitation and inhibition. The slow eigenvalue is located at $(\gamma\mu_E p_E - \gamma\mu_I p_I - 1)/\tau$, where μ_E and μ_I are the magnitudes of the coupling strengths for excitation and inhibition respectively, p_E and p_I are the respective connection probabilities, and, as before, τ is the intrinsic decay time-constant and γ is the slope of the *f*–*I* curve (see SI, Section 9). If this difference between excitation and inhibition closely balances the intrinsic decay then the network will show long timescales. In Figure 4*C* we show how the power spectrum of a network with 80% excitatory and 20% inhibitory connections can reproduce the observed power spectra.

The low-frequency component of the ECoG power spectrum has been shown to differ between arousal states (i.e., waking vs. sleep) (He et al. 2010) and to change upon task initiation (He et al. 2010; He 2011; Ciuciu et al. 2012). We next investigate manipulations of the model that may underlie such state-dependent changes in the shape of the low-frequency power spectrum.

Correlations in the Input Preferentially Drive Slow Timescales

The eigenvector corresponding to a timescale determines not only the distribution of that mode across the network, but also how much that mode is activated in response to a given profile of input. Given a particular pattern of input across the network, the correlation of this input pattern with an eigenvector determines how strongly the corresponding temporal mode is driven (this is approximately true, but see SI, Section 5 for a more precise statement). This corresponds to the intuition that input whose spatial distribution resembles a particular eigenvector should preferentially activate the temporal mode corresponding to that eigenvector.

The slow and fast modes have different distributions, and thus are differently driven by various inputs (see SI, Eq. 18 for the power spectrum). The slow mode is shared across the network and is driven by the component of the input that is common between nodes (see SI, Section 6). By contrast, input that is uncorrelated between nodes drives the slow network mode incoherently, with some nodes contributing positively and others negatively, so that the net effect is small. As a consequence, a random recurrent network architecture generically transforms correlations in input across nodes into long temporal correlations in network activity. In Figure 5*B* we show how the power spectrum of node activity depends on the degree of correlation in the input across the network (recall that the power spectra in Figure 3 are for uncorrelated input). In particular, we note that a decorrelation of input across neurons would lead to a reduction in low-frequency power, as observed in ECoG power upon task-initiation (He et al. 2010), and shown in Figure 5*C*.

Distance-Dependent Connection Probability Changes the Slope of the Low-Frequency Power Spectrum

We have assumed that the nodes in the network are connected to each other with equal probability and mean weight. However, networks of neurons that are widely distributed in space typically have a distance-dependence in connection probability and number: several studies have concluded that neural connectivity is primarily local and, despite notable exceptions, tends to decay with distance both within a cortical area and between cortical areas (Destexhe et al. 1999; Ercsey-Ravasz et al. 2013; Markov et al. 2014). We now consider model networks with nodes that have some underlying spatial location and whose connection strength decays exponentially with distance.

In Figure 6*A*, we show the eigenvalue distributions of 3 such networks with progressively sharper connectivity profiles. In contrast to the completely random network of Figure 3, these networks contain a number of intermediate eigenvalues between the slow shared mode and the cluster of modes around the single-node timescale. As the decay of connections with distance becomes sharper, the number of intermediate eigenvalues increases; this can be understood by noting that the positions of the eigenvalues are approximately given by the Fourier transform of the connectivity profile (see SI, Section 10), and hence networks with sharply localized connectivity will have eigenvalues that are more spread out.

In Figure 6*B* we show the effect of distance-dependent connectivity on the network power spectrum. Heuristically, the intermediate eigenvalues contribute Lorentzian functions with knee frequencies located in the low-frequency part of the power spectrum. These combine to produce a shallower low-frequency slope. As the distance-dependent decay of connectivity becomes steeper there are more such intervening modes, and the slope of the low-frequency network power spectrum continues to become shallower, leading to a scaling of power with frequency that is closer to $1/f$ (as seen in the light green trace of Fig. 6*B*). Thus, networks with predominantly local connectivity could underlie experimental observations of $1/f$ power spectra in recordings (Bedard et al. 2006; Bedard and Destexhe 2009; Dehghani et al. 2010), and different distance-dependent profiles of connectivity could explain differences in the slope of low-frequency power spectra between subjects, regions of the cortex or arousal states.

Clustered Network Architectures

Thus far we have treated nodes in our network as single entities with no internal structure. While it is possible that the nodes correspond to single neurons, the node timescales we observe are on the order of hundreds of milliseconds. This is

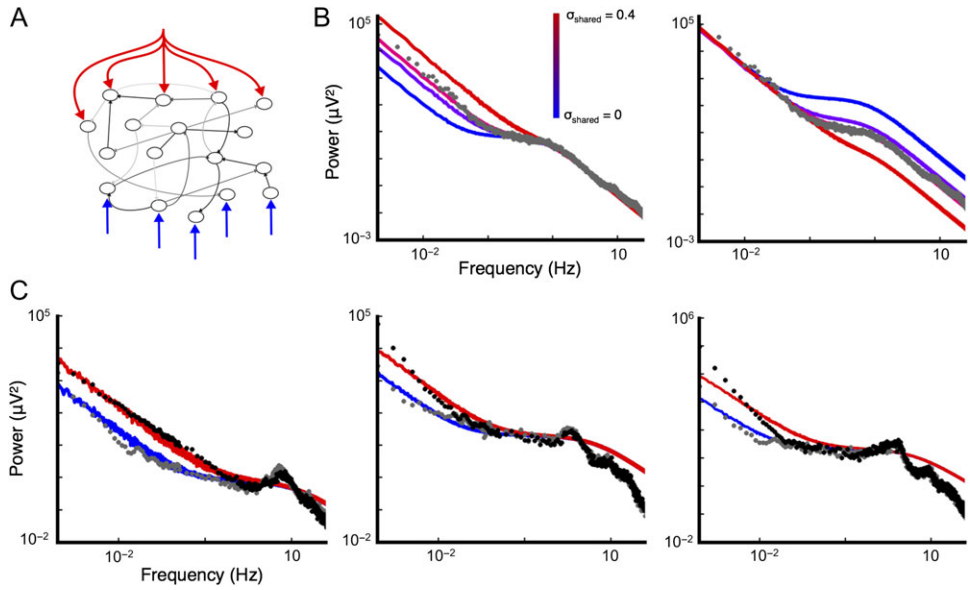

Figure 5. The network converts shared input into network activity with long temporal correlations. (*A*) Schematic of a random network with nodes that receive both shared input (red) and uncorrelated input (blue). (*B*) Power spectra for network activity in response to different fractions of correlated input. Left panel shows that correlated input leads to an increase in low-frequency power in the network, while right panel shows normalized power spectra. The average power spectrum from Patient 3 is shown as dark gray circles, for comparison. To highlight the role of correlated input in driving the slow mode, we average over a smaller fraction of network nodes. Thus, the blue trace (without input correlations) reflects the fast modes to a greater extent than the data, but this can be compensated for by more correlation in the input. σ^2_{shared} is the variance of the common input; the variance of the remaining input (uncorrelated across nodes) is chosen so that total variance is constant (see SI, Section 8). Note that the power spectrum is still well-fit by the sum of 2 Lorentzians, with the amplitudes depending on the degree of correlation (SI, Eq. 18). (*C*) Three electrodes showing strong task modulation along with Lorentzian fits. The same network is fit to both rest and task conditions, and only σ^2_{shared} is changed to move from rest to task power spectrum. For the 3 fits, α = 1/292, 1/1186, and 1/1483, respectively (N = 292, 1186, 1483), and τ = 15.6, 25.3, and 26.1 ms, respectively.

longer than membrane time constants and most synaptic time constants; however, it is within the range of other long cellular time constants (Carter and Wang 2007; Zhang and Seguela 2010; Letzkus et al. 2011), and we consider these further in the Discussion. Alternatively, the nodes could correspond to cell assemblies or clusters of neurons. A number of studies suggest that cortical connectivity is clustered at multiple spatial scales (Mountcastle 2003; Song et al. 2005; Perin et al. 2011), that these clusters may form functional units (Yoshimura et al. 2005; Ko et al. 2011), and that model networks with clustering can show long timescales and high variability (Rubinov et al. 2011; Litwin-Kumar and Doiron 2012). We extend our model to a clustered network where individual neurons in each cluster show faster timescales (on the order of milliseconds) and the timescales of each cluster emerge from recurrent interactions. The resulting architecture is thus hierarchical: individual neurons form clusters via recurrent interactions and the clusters further interact to produce the very long network timescales.

The eigenvalue spectrum of a network with such a clustered structure is shown in Figure 7*B*. For a network with N clusters, the eigenvalue spectrum shows a single slow mode near 0 (red circle) and $N - 1$ faster modes distributed around the time-constant of a single cluster (blue circles). Thus, the long timescale behavior is the same as before. However, the eigenvalue spectrum also shows a number of much faster modes clustered around the intrinsic time-constant of a single neuron (black circles). In the lower panel of Figure 7*B* we highlight these 2 regions of the eigenvalue spectrum, revealing the signature of the underlying hierarchical architecture.

In Figure 7*C* we show the power spectrum of the average activity of a cluster in this network, after averaging across the individual neurons. This power spectrum is dominated by the emergent slow timescale and by the timescale of the clusters. The contribution of the very fast neural timescales is small (Supplementary Fig. 2). They originate locally and are only weakly correlated with each other and thus their contribution is strongly attenuated by averaging over the spatial scale of the cluster. Moreover, these fast timescales are on the order of milliseconds, and thus any contribution they do make is only visible at high frequencies.

As shown in Figure 2, the knee frequencies we fit vary across electrodes and between subjects. In the model, the knee frequency corresponds to the timescale of a node or local cluster, and a variation in knee frequency suggests that the network nodes underlying each electrode show different timescales. These differences could emerge from spatial variation in the cellular and synaptic time constants of individual neurons, in the strength of recurrent interactions between the neurons and in the characteristic size of a cluster. In Figure 7*D*, we show how the location of the knee frequency (i.e., the timescale of a cluster) depends on these parameters.

Discussion

Human ECoG power spectra below ~4 Hz show evidence of simple linear dynamics dominated by a slow and a fast mode. We demonstrate how these can reflect an underlying recurrent network with few assumptions on the connectivity: connections are random and net excitatory so as to balance the intrinsic decay of node activity.

Electric field potentials are thought to result from a linear sum of transmembrane currents, weighted by their inverse distance from the electrode (Nunez and Srinivasan 2006).

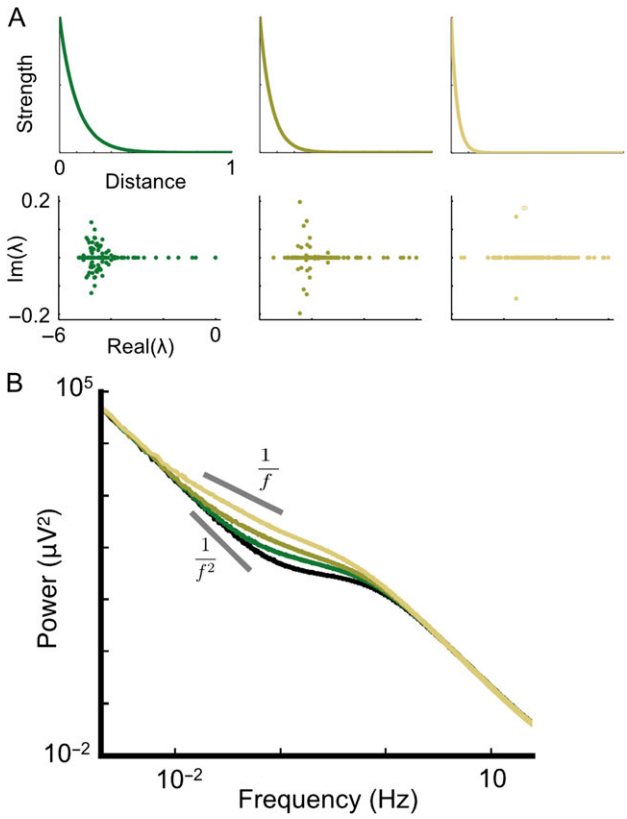

Figure 6. Network endowed with distance-dependent connectivity yields shallower power spectra. (*A*) Connectivity profile of 3 networks with increasingly sharp decay of connection strength with distance (top), and the corresponding eigenvalue spectra (bottom). (*B*) Power spectra for the 3 networks shown in (*A*) (in successively lighter shades of green) along with the power spectrum from Figure 3, for comparison (shown in black).

We assume that the electric field potentials are dominated by synaptic currents (and the corresponding return currents) ((Buzsáki et al. 2012; Einevoll et al. 2013), but also see (Reimann et al. 2013) for an opposing argument). For many neurons the dependence of firing rate on input is approximately threshold-linear over a wide range (Ahmed et al. 1998; Ermentrout 1998; Wang 1998; Chance et al. 2002), and linear networks are common models for the dynamics of neural circuits (Dayan and Abbott 2001; Shriki et al. 2003; Vogels et al. 2005; Rajan and Abbott 2006; Ganguli et al. 2008; Murphy and Miller 2009). Thus, we assume that neural firing rate is a linear function of input current. This is a strong simplification, but we think it is justified both in terms of reproducing empirical power spectra without many parameters and because it provides for theoretical understanding, suggesting putative explanations for the different regions of the power spectrum and how they change with network structure and input.

Assuming that firing rate is a linear function of current predicts a relationship between firing rate and electric field potential, at least at low frequencies. This is supported by observations that the slow cortical potential (SCP) (<5 Hz activity) reflects different states of cortical excitability, with surface-recorded negative shifts indexing enhanced cortical excitability (Rockstroh et al. 1989; Birbaumer et al. 1990; He and Raichle 2009). The negative shift of SCP is also correlated with higher multiunit activity (Rebert 1973). Finally, the phase of SCP modulates broadband gamma power (He 2014), which in turn is correlated with firing rate (Manning et al. 2009). The relationship between broadband power and firing rate also suggests that the power spectrum of broadband power will reflect the shape of the electric field potential, at least at low frequencies; in particular, if the broadband power to firing rate relationship is close to linear, then the broadband power should show knees at the same locations as the field potential. Future work could use simultaneous recordings of firing rate and ECoG to test the *f–I* relationship we used here and extend the model. From the ECoG data, both SCP and broadband power can be extracted, and a more comprehensive model accounting for both could be developed. Technically, this could be done by simultaneous Utah array and ECoG (Hochberg et al. 2006; Truccolo et al. 2011), or simultaneous Neurogrid and ECoG (Khodagholy et al. 2015) in animal models or human patients.

Our model for the generation of the electric potential from neural activity is simpler than models for LFP (Mazzoni et al. 2008, 2015; Lindén et al. 2011), but shares the same basic assumptions. Most of these models assume that the field potential is a distance-weighted sum of synaptic currents, but consider spatially extended or spiking neuron models. Such models are necessary to predict the spatial distribution of LFP (e.g., across layers), and high-frequency activity, and our model only seeks to predict the signal at the electrode, with a focus on low-frequency activity. An interesting future direction is to extend the model to simultaneously model multiple spatial scales, such as both LFP and ECoG.

The data contain very long correlation times (seen in the low-frequency power). In the model, this slow timescale emerges when recurrent excitatory interactions closely balance the intrinsic decay of activity at each node (or decay plus inhibition). Thus, the fitted model is near a bifurcation point, such as those seen at the appearance or disappearance of a fixed point or attractor, and the behavior of the model is very sensitive to the degree of this balance (i.e., the proximity to the bifurcation point), which is determined by the parameter $p\mu_{conn}$. We find these long time-constants empirically and do not propose how recurrent excitation (or the difference between excitation and inhibition) can be driven to this point. However, several mechanisms have been proposed (Levina et al. 2007; Magnasco et al. 2009; Chialvo 2010; Millman et al. 2010; Rubinov et al. 2011; Moretti and Muñoz 2013). Long correlation times are seen in systems near phase transitions (Stanley 1999; Sethna 2006), leading to speculation that the brain is perched at a critical point (Beggs and Plenz 2003; Plenz and Thiagarajan 2007; Beggs and Timme 2012; Deco and Jirsa 2012; Priesemann et al. 2014; Bellay et al. 2015; Roberts et al. 2015), and to suggestions that proximity to criticality provides desirable functional properties (Langton 1990; Mitchell et al. 1993; Kinouchi and Copelli 2006; Mora and Bialek 2011; Shew and Plenz 2013). Interestingly, both long temporal correlations and the amount of total fluctuations are suppressed upon task initiation (He et al. 2010; He 2011, 2013; Ciuciu et al. 2012), suggesting that task performance may shift the system away from criticality (Deco and Jirsa 2012; Fagerholm et al. 2015).

A number of factors besides network activity could contribute to the low-frequency component of the power spectrum. One possibility is global fluctuations in excitability (Scholvinck et al. 2010), such as might arise from slow changes in brain state or neuromodulation. Another is very slow cellular processes, which may be linked to neuromodulation or emerge locally. A third possibility is that neural networks inherit part of their low-frequency structure from slow fluctuations in the input. The model can be extended to explicitly incorporate

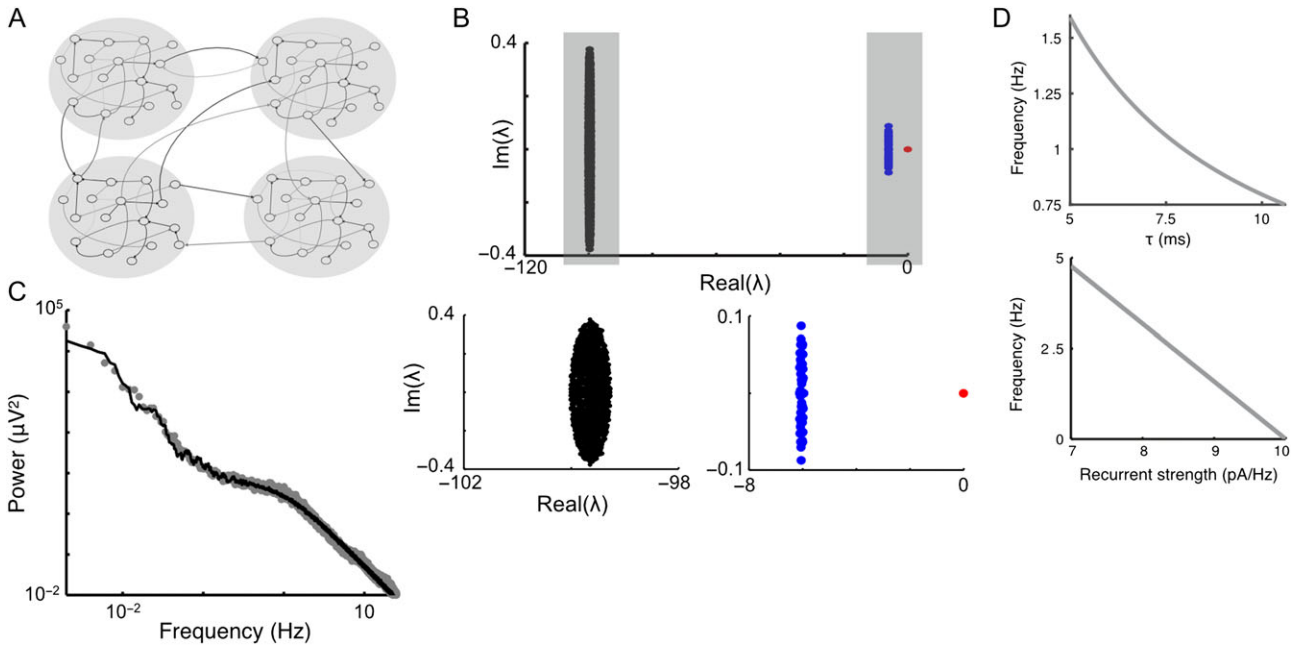

Figure 7. Power spectrum of a network with nodes which are themselves clusters of sub-nodes. (*A*) Schematic of the network, with 4 clusters shown. (*B*) Eigenvalue spectrum of the network. Top panel shows the full eigenvalue spectrum while the 2 bottom panels highlight the eigenvalues in the 2 gray regions. Note the hierarchical organization of the eigenvalue spectrum: the black eigenvalues reflect the timescales of individual nodes; the blue eigenvalues reflect within-cluster recurrent connections; and the red eigenvalue emerges from connections between clusters. (*C*) Power spectrum of network activity (black) along with data from Patient 3 (grey filled circles). (*D*) Dependence of the knee frequency on intrinsic time-constant of sub-node (top panel) and on the recurrent connection strength for within-cluster connections (bottom panel). The recurrent input within a cluster is the product of connection probability, recurrent connection strength and the number of sub-nodes (i.e., size of a cluster). Increasing the intrinsic time-constant or the recurrent strength makes the network dynamics slower and thus the knee in the power spectrum shifts to lower frequencies.

these possibilities. The contributions of various factors can be constrained both by investigating the spatial and functional specificity of low-frequency activity (He et al. 2008) and by manipulations that differentially affect network-generated slow fluctuations, such as by disrupting recurrent excitation or enhancing inhibition. These could include targeted activation or inhibition of neural sub-types. Note that interventions that disrupt network activity may be unable to distinguish slow network timescales from those that are inherited from an input. If these long correlation times are inherited from an external input, then whitening the low-frequency structure of the input would remove these timescales in the electric potential. On the other hand, if these timescales reflect input from another set of neurons or brain region, then resolving these mechanisms will require simultaneous recording of both sets of neurons.

Multiple model features can be understood from the link between long timescales and recurrent excitatory interactions. The long timescales that emerge from internode interactions are spatially distributed and hence correlated across nodes, while faster timescales are more local. This may explain why correlations in low-frequency activity are more widely distributed than correlations in high-frequency activity (von Stein and Sarnthein 2000; Buzsáki 2006). In general, network-level activity is correlated across nodes and will become more visible after spatial averaging, such as during field potential recordings, while activity that emerges more locally will be suppressed. Thus, the model predicts that recordings that average activity over large numbers of neurons will be dominated by slower timescales (Fig. 3*E*). In particular, LFP should show comparatively less power at very low frequencies than ECoG, which in turn should show less very low-frequency power than EEG. These observations could be tested in DC-coupled LFP (Kahn et al. 2013; Pan et al. 2013) and EEG (Birbaumer et al. 1990) recordings.

Our model suggests potential mechanisms for the decrease in autocorrelation (as captured by the low-frequency power-law exponent β) in ECoG and fMRI recordings upon task initiation (He et al. 2010; He 2011; Ciuciu et al. 2012). As shown in Figure 5, a reduction of shared inputs among nodes leads to a decrease of low-frequency power of network fluctuations, supporting a suggestion (He 2011) that task-induced changes may result from neurons in the local network becoming more independent (Poulet and Petersen 2008). This decorrelation could result from nodes receiving more heterogeneous input or from an active top-down process, such as attentional decorrelation (Cohen and Maunsell 2009; Mitchell et al. 2009). However, the studies just mentioned involve tasks that do not require much integration of input, and a task that involved integrating information over multiple modalities or long periods of time may lead to an increase in correlated task-related input.

Adding a decay of connection strength with distance caused the low-frequency power spectrum slope to become shallower. Thus, differences in connectivity structure within the same model can account for observed divergences in low-frequency power spectra, such as in the studies of Destexhe et al., 1999 and Dehghani et al., 2010 which found slopes of −1 in the low-frequency power spectra of cat cortical LFP and human EEG, respectively. Given observations of reduced long-range effective connectivity in the human brain during slow-wave sleep (Massimini et al. 2005), differences in long-range connectivity might also provide a mechanistic explanation for shallower power spectra in the <0.1 Hz range during slow-wave sleep compared with the awake state (He et al. 2010). Furthermore, while a power spectrum that scales as $1/f$ is often taken to

signify self-organization (Bak et al. 1987; Turcotte 1999), we find that sharply decaying connectivity produces a spread of exponential modes; as previously shown, summing such dispersed modes can produce a spectrum that scales as $1/f$ without invoking additional physical processes (Bell 1960; Milotti 1995; Wagenmakers et al. 2004; Erland and Greenwood 2007). More generally, our model suggests that the low-frequency power spectrum is sensitive to features of network organization (such as degree of averaging, connectivity decay length, ratio of excitation to inhibition, and correlations in the input) and could be a probe of network reconfiguration.

The knee frequencies in the average empirical power spectra (Fig. 1*D*) are located at 0.49, 0.55, 0.81, 1.10, and 3.47 Hz, respectively, corresponding to timescales of 325, 289, 196, 145, and 46 ms (timescale is $1/2\pi f_{\text{fast}}$). This frequency varies dramatically between subjects and electrodes, but contains spatial structure: 4 out of 5 patients show evidence of a gradient across electrodes and, at least in Patients #1 and #3, frontal areas tend to exhibit slower timescales. This may reflect a hierarchy of cortical timescales, with sensory areas processing information rapidly, whereas cognitive areas integrate information over time (Honey et al. 2012). Indeed the timescales of the knee frequencies are similar to those observed in small fluctuations across cortical areas in the macaque, perhaps suggesting a common origin, and those timescales were found to be hierarchically structured (Murray et al. 2014). We also note that while 4 patients show knee frequencies near 1 Hz, Patient #5 shows a faster frequency near 3.5 Hz. While our sample size is small, Patient #5 is older and the difference may reflect an age-related shift in electrophysiological activity towards higher frequencies (McIntosh et al. 2010).

In the model, the knee frequency is determined by the timescales of individual nodes, and the model predicts that this should be a relatively stable property of the local circuit, unaffected by task or network reorganization. If the nodes correspond to neurons then these might be the timescales of a slow synaptic or cellular process such as the NMDA pathway (Wang 1999), metabotropic glutamate receptors (Zhang and Seguela 2010), cholinergic modulation (Letzkus et al. 2011), or endocannabinoid signaling (Carter and Wang 2007), which may vary across electrodes and subjects. For instance, time constants for synaptic transmission and single neuron dynamics may differ between sensory and association areas (Wang et al. 2008; Pereira and Wang 2015). Alternately, the nodes might correspond to neural assemblies or clusters and the knee frequency would correspond to the timescales of these clusters, determined by local timescales and recurrent interaction within a cluster (Fig. 7). Modeling work suggests that a gradient of recurrent connection strengths across cortical areas could produce differences in these timescales (Chaudhuri et al. 2015). Manipulations that disrupt local excitation could help distinguish these possibilities.

Above ~80 Hz, ECoG power spectra have a slope steeper than 2 (Miller et al. 2009a; He et al. 2010). As observed in Miller et al. (2009a), this transition points to an even faster timescale in the data and suggests fitting the high-frequency data with a product of 2 Lorentzians. This produces a power spectrum that transitions from $1/f^2$ scaling to $1/f^4$ (Fig. 8). The very short timescale (values in Fig. 8) could emerge from fast timescales in neural input possibly imposed by synaptic time constants (Miller et al. 2009a), from a fast timescale in the output (perhaps reflecting a neuronal membrane time constant, especially in the high-conductance state (Destexhe et al. 2003; Koch et al. 1996)), or from dendritic filtering (Linden et al. 2010; Einevoll et al. 2013). Extracellular tissue filtering might also play a role

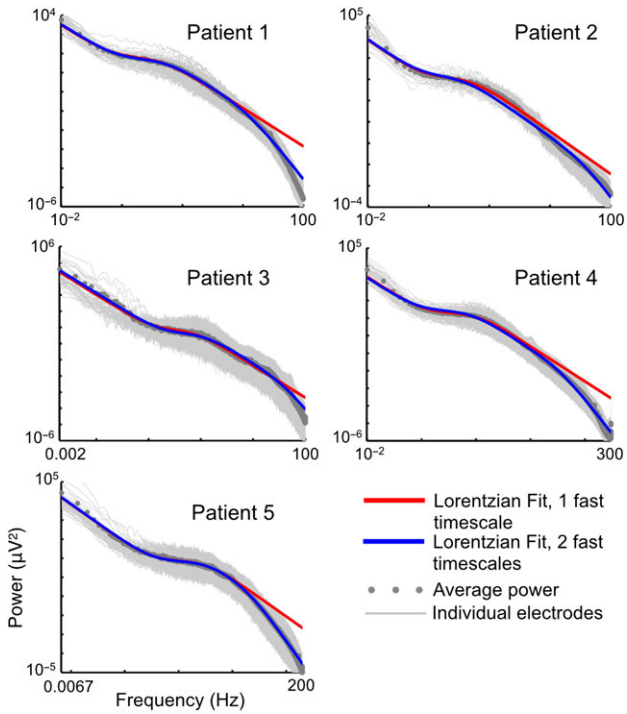

Figure 8. Adding a fast filtering timescale accounts for the high-frequency structure of observed power spectra. The light grey traces are recordings from each electrode while the dark grey circles are the averages across all electrodes. Red traces are the original fits with a sum of 2 Lorentzian functions, while blue traces are fits using a fourth free parameter, corresponding to a timescale on the order of milliseconds. The data is fit to the frequencies below 50 Hz. The high transition frequencies are 13.03, 40.68, 40.50, 37.42, and 21.89 Hz, respectively, corresponding to timescales of 12.21, 3.91, 3.93, 4.25, and 7.27 ms. Note that the study of He et al. (2010) was intended to examine the low-frequency range, and thus the high-frequency cutoff is comparatively low; however, a similar shape for the high-frequency power spectrum was observed up to ~500 Hz by Miller et al. (2009a).

(Bedard et al. 2006; Dehghani et al. 2010), although this effect remains controversial (Logothetis et al. 2007). Modeling these effects by assuming that the input to or activity from our model is correlated with a timescale on the order of milliseconds extends the fits into the high-frequency range. The model predicts that the slope below this high-frequency transition should be correlated with the slope above it: if the exponent of the slope below is $-\beta$ then the exponent of the higher frequency slope should be $-(2+\beta)$. However, it suggests no relationship between the locations of the 2 knees in the power spectrum.

In summary, our model provides a parsimonious framework for interpreting broadband, arrhythmic field potentials recorded by ECoG and LFP. The model links macroscopic arrhythmic field potentials with underlying neural network dynamics, and shows that features of the broadband power spectrum may be diagnostic of the underlying network architecture. This framework may contribute to a unified understanding of previous studies and to generating and testing new hypotheses about the relationship between broadband power spectra and network organization.

Authors' Contributions

R.C., B.J.H., and X.-J.W. designed research; R.C. performed research and analyzed data; R.C., B.J.H., and X.-J.W. wrote the article.

Supplementary Material

Supplementary data is available at *Cerebral Cortex* online.

Funding

Office of Naval Research (N00014-13-1-0297 to X.J.W.); the National Institutes of Health (Grant R01MH062349 to X.J.W.); and by the intramural research program of the National Institutes of Health/National Institute of Neurological Disorders and Stroke, Leon Levy Foundation, and Klingenstein-Simons Fellowship (to B.J.H.).

Notes

We thank Alberto Bernacchia, John Murray, Francis Song, and Guangyu Yang for discussions. The authors declare no competing financial interests. *Conflict of Interest*: None declared.

References

Ahmed B, Anderson J, Douglas R, Martin K, Whitteridge D. 1998. Estimates of the net excitatory currents evoked by visual stimulation of identified neurons in cat visual cortex. Cereb Cortex. 8:462–476.

Bak P, Tang C, Wiesenfeld K. 1987. Self-organized criticality: an explanation of the 1/f noise. Phys Rev Lett. 59:381.

Bedard C, Destexhe A. 2009. Macroscopic models of local field potentials and the apparent 1/f noise in brain activity. Biophys J. 96:2589–2603.

Bedard C, Kroger H, Destexhe A. 2006. Does the 1/f frequency scaling of brain signals reflect self-organized critical states? Phys Rev Lett. 97:118102.

Beggs JM, Plenz D. 2003. Neuronal avalanches in neocortical circuits. J Neurosci. 23:11167–11177.

Beggs JM, Timme N. 2012. Being critical of criticality in the brain. Front Physiol. 3:163.

Bell DA. 1960. Electrical noise. Princeton, NJ: Van Nostrand.

Bellay T, Klaus A, Seshadri S, Plenz D. 2015. Irregular spiking of pyramidal neurons organizes as scale-invariant neuronal avalanches in the awake state. Elife. 4:e07224.

Birbaumer N, Elbert T, Canavan A, Rockstroh B. 1990. Slow potentials of the cerebral cortex and behavior. Physiol Rev. 70:1–41.

Bouchard KE, Mesgarani N, Johnson K, Chang EF. 2013. Functional organization of human sensorimotor cortex for speech articulation. Nature. 495:327–332.

Buzsáki G. 2006. Rhythms of the brain. Oxford: Oxford University Press.

Buzsáki G, Anastassiou CA, Koch C. 2012. The origin of extracellular fields and currents—EEG, ECoG, LFP and spikes. Nat Rev Neurosci. 13:407–420.

Buzsáki G, Wang XJ. 2012. Mechanisms of gamma oscillations. Annu Rev Neurosci. 35:203–225.

Carter E, Wang XJ. 2007. Cannabinoid-mediated disinhibition and working memory: dynamical interplay of multiple feedback mechanisms in a continuous attractor model of prefrontal cortex. Cereb Cortex. 17(Suppl 1):16–26.

Chance FS, Abbott LF, Reyes AD. 2002. Gain modulation from background synaptic input. Neuron. 35:773–782.

Chaudhuri R, Knoblauch K, Gariel MA, Kennedy H, Wang XJ. 2015. A large-scale circuit mechanism for hierarchical dynamical processing in the primate cortex. Neuron. 88:419–431.

Chialvo DR. 2010. Emergent complex neural dynamics. Nat Phys. 6:744–750.

Ciuciu P, Varoquaux G, Abry P, Sadaghiani S, Kleinschmidt A. 2012. Scale-free and multifractal time dynamics of fMRI signals during rest and task. Front Physiol. 3:186.

Cohen MR, Maunsell JH. 2009. Attention improves performance primarily by reducing interneuronal correlations. Nat Neurosci. 12:1594–1600.

Crone NE, Miglioretti DL, Gordon B, Lesser RP. 1998. Functional mapping of human sensorimotor cortex with electrocorticographic spectral analysis. II. Event-related synchronization in the gamma band. Brain. 121:2301–2315.

Dayan P, Abbott LF. 2001. Theoretical neuroscience. Cambridge, MA: The MIT Press.

Deco G, Jirsa VK. 2012. Ongoing cortical activity at rest: criticality, multistability, and ghost attractors. J Neurosci. 32:3366–3375.

Dehghani N, Bedard C, Cash SS, Halgren E, Destexhe A. 2010. Comparative power spectral analysis of simultaneous electroencephalographic and magnetoencephalographic recordings in humans suggests non-resistive extracellular media. J Comput Neurosci. 29:405–421.

Destexhe A, Contreras D, Steriade M. 1999. Spatiotemporal analysis of local field potentials and unit discharges in cat cerebral cortex during natural wake and sleep states. J Neurosci. 19:4595–4608.

Destexhe A, Rudolph M, Pare D. 2003. The high-conductance state of neocortical neurons in vivo. Nat Rev Neurosci. 4:739–751.

Einevoll GT, Kayser C, Logothetis NK, Panzeri S. 2013. Modelling and analysis of local field potentials for studying the function of cortical circuits. Nat Rev Neurosci. 14:770–785.

Ercsey-Ravasz M, Markov NT, Lamy C, Van Essen DC, Knoblauch K, Toroczkai Z, Kennedy H. 2013. A predictive network model of cerebral cortical connectivity based on a distance rule. Neuron. 80:184–197.

Erland S, Greenwood PE. 2007. Constructing $1/\omega^{\alpha}$ noise from reversible Markov chains. Phys Rev E Stat Nonlin Soft Matter Phys. 76:031114.

Ermentrout B. 1998. Linearization of F-I curves by adaptation. Neural Comput. 10:1721–1729.

Fagerholm ED, Lorenz R, Scott G, Dinov M, Hellyer PJ, Mirzaei N, Leeson C, Carmichael DW, Sharp DJ, Shew WL, et al. 2015. Cascades and cognitive state: focused attention incurs subcritical dynamics. J Neurosci. 35:4626–4634.

Freeman WJ, Zhai J. 2009. Simulated power spectral density (PSD) of background electrocorticogram (ECoG). Cogn Neurodyn. 3:97–103.

Fries P. 2009. Neuronal gamma-band synchronization as a fundamental process in cortical computation. Annu Rev Neurosci. 32:209–224.

Ganguli S, Bisley JW, Roitman JD, Shadlen MN, Goldberg ME, Miller KD. 2008. One-dimensional dynamics of attention and decision making in LIP. Neuron. 58:15–25.

He BJ. 2011. Scale-free properties of the functional magnetic resonance imaging signal during rest and task. J Neurosci. 31:13786–13795.

He BJ. 2013. Spontaneous and task-evoked brain activity negatively interact. J Neurosci. 33:4672–4682.

He BJ. 2014. Scale-free brain activity: past, present, and future. Trends Cogn Sci. 18:480–487.

He BJ, Raichle ME. 2009. The fMRI signal, slow cortical potential and consciousness. Trends Cogn Sci. 13:302–309.

He BJ, Snyder AZ, Zempel JM, Smyth MD, Raichle ME. 2008. Electrophysiological correlates of the brain's intrinsic large-scale functional architecture. Proc Natl Acad Sci USA. 105:16039–16044.

He BJ, Zempel JM, Snyder AZ, Raichle ME. 2010. The temporal structures and functional significance of scale-free brain activity. Neuron. 66:353–369.

Hochberg LR, Serruya MD, Friehs GM, Mukand JA, Saleh M, Caplan AH, Branner A, Chen D, Penn RD, Donoghue JP. 2006. Neuronal ensemble control of prosthetic devices by a human with tetraplegia. Nature. 442:164–171.

Honey CJ, Thesen T, Donner TH, Silbert LJ, Carlson CE, Devinsky O, Doyle WK, Rubin N, Heeger DJ, Hasson U. 2012. Slow cortical dynamics and the accumulation of information over long timescales. Neuron. 76:423–434.

Jensen O, Bonnefond M, VanRullen R. 2012. An oscillatory mechanism for prioritizing salient unattended stimuli. Trends Cogn Sci. 16:200–206.

Kahn I, Knoblich U, Desai M, Bernstein J, Graybiel A, Boyden E, Buckner R, Moore C. 2013. Optogenetic drive of neocortical pyramidal neurons generates fMRI signals that are correlated with spiking activity. Brain Res. 1511:33–45.

Khodagholy D, Gelinas JN, Thesen T, Doyle W, Devinsky O, Malliaras GG, Buzsáki G. 2015. NeuroGrid: recording action potentials from the surface of the brain. Nat Neurosci. 18: 310–315.

Kinouchi O, Copelli M. 2006. Optimal dynamical range of excitable networks at criticality. Nat Phys. 2:348–351.

Ko H, Hofer SB, Pichler B, Buchanan KA, Sjöström PJ, Mrsic-Flogel TD. 2011. Functional specificity of local synaptic connections in neocortical networks. Nature. 473:87–91.

Koch C, Rapp M, Segev I. 1996. A brief history of time (constants). Cereb Cortex. 6:93–101.

Langton CG. 1990. Computation at the edge of chaos: phase transitions and emergent computation. Physica D. 42:12–37.

Leopold DA, Murayama Y, Logothetis NK. 2003. Very slow activity fluctuations in monkey visual cortex: implications for functional brain imaging. Cereb Cortex. 13:422–433.

Letzkus JJ, Wolff SB, Meyer EM, Tovote P, Courtin J, Herry C, Luthi A. 2011. A disinhibitory microcircuit for associative fear learning in the auditory cortex. Nature. 480:331–335.

Levina A, Herrmann JM, Geisel T. 2007. Dynamical synapses causing self-organized criticality in neural networks. Nat Phys. 3:857–860.

Linden H, Pettersen KH, Einevoll GT. 2010. Intrinsic dendritic filtering gives low-pass power spectra of local field potentials. J Comput Neurosci. 29:423–444.

Lindén H, Tetzlaff T, Potjans TC, Pettersen KH, Grün S, Diesmann M, Einevoll GT. 2011. Modeling the spatial reach of the LFP. Neuron. 72:859–872.

Litwin-Kumar A, Doiron B. 2012. Slow dynamics and high variability in balanced cortical networks with clustered connections. Nat Neurosci. 15:1498–1505.

Logothetis NK, Kayser C, Oeltermann A. 2007. In vivo measurement of cortical impedance spectrum in monkeys: implications for signal propagation. Neuron. 55:809–823.

Magnasco MO, Piro O, Cecchi GA. 2009. Self-tuned critical anti-Hebbian networks. Phys Rev Lett. 102:258102.

Manning JR, Jacobs J, Fried I, Kahana MJ. 2009. Broadband shifts in local field potential power spectra are correlated with single-neuron spiking in humans. J Neurosci. 29:13613–13620.

Manning JR, Sperling MR, Sharan A, Rosenberg EA, Kahana MJ. 2012. Spontaneously reactivated patterns in frontal and temporal lobe predict semantic clustering during memory search. J Neurosci. 32:8871–8878.

Markov NT, Ercsey-Ravasz MM, Ribeiro Gomes AR, Lamy C, Magrou L, Vezoli J, Misery P, Falchier A, Quilodran R, Gariel MA, et al. 2014. A weighted and directed interareal connectivity matrix for macaque cerebral cortex. Cereb Cortex. 24:17–36.

Massimini M, Ferrarelli F, Huber R, Esser SK, Singh H, Tononi G. 2005. Breakdown of cortical effective connectivity during sleep. Science. 309:2228–2232.

Mazzoni A, Lindén H, Cuntz H, Lansner A, Panzeri S, Einevoll GT. 2015. Computing the local field potential (LFP) from integrate-and-fire network models. PLoS Comput Biol. 11:e1004584.

Mazzoni A, Panzeri S, Logothetis NK, Brunel N. 2008. Encoding of naturalistic stimuli by local field potential spectra in networks of excitatory and inhibitory neurons. PLoS Comput Biol. 4:e1000239.

McIntosh AR, Kovacevic N, Lippe S, Garrett D, Grady C, Jirsa V. 2010. The development of a noisy brain. Arch Ital Biol. 148:323–337.

Miller KJ, Sorensen LB, Ojemann JG, den Nijs M. 2009a. Power-law scaling in the brain surface electric potential. PLoS Comput Biol. 5:e1000609.

Miller KJ, Zanos S, Fetz EE, den Nijs M, Ojemann JG. 2009b. Decoupling the cortical power spectrum reveals real-time representation of individual finger movements in humans. J Neurosci. 29:3132–3137.

Millman D, Mihalas S, Kirkwood A, Niebur E. 2010. Self-organized criticality occurs in non-conservative neuronal networks during Up states. Nat Phys. 6:801–805.

Milotti E. 1995. Linear processes that produce 1/f or flicker noise. Phys Rev E Stat Phys Plasmas Fluids Relat Interdiscip Topics. 51:3087–3103.

Milstein J, Mormann F, Fried I, Koch C. 2009. Neuronal shot noise and Brownian $1/f^2$ vior in the local field potential. PLoS One. 4:e4338.

Mitchell JF, Sundberg KA, Reynolds JH. 2009. Spatial attention decorrelates intrinsic activity fluctuations in macaque area V4. Neuron. 63:879–888.

Mitchell M, Hraber P, Crutchfield JP. 1993. Revisiting the edge of chaos: evolving cellular automata to perform computations. Complex Sys. 7:89–130.

Mora T, Bialek W. 2011. Are biological systems poised at criticality? J Stat Phys. 144:268–302.

Moretti P, Muñoz MA. 2013. Griffiths phases and the stretching of criticality in brain networks. Nat Commun. 4:2521.

Mountcastle VB. 2003. Introduction. Computation in cortical columns. Cereb Cortex. 13:2–4.

Murphy BK, Miller KD. 2009. Balanced amplification: a new mechanism of selective amplification of neural activity patterns. Neuron. 61:635–648.

Murray JD, Bernacchia A, Freedman DJ, Romo R, Wallis JD, Cai X, Padoa-Schioppa C, Pasternak T, Seo H, Lee D, et al. 2014. A hierarchy of intrinsic timescales across primate cortex. Nat Neurosci. 17:1661–1663.

Nunez PL, Srinivasan R. 2006. Electric fields of the brain: the neurophysics of EEG. Oxford: Oxford University Press.

Onton JA, Makeig S. 2009. High-frequency broadband modulation of electroencephalographic spectra. Front Hum Neurosci. 3:61.

Ossandón T, Jerbi K, Vidal JR, Bayle DJ, Henaff MA, Jung J, Minotti L, Bertrand O, Kahane P, Lachaux JP. 2011. Transient suppression of broadband gamma power in the default-mode network is correlated with task complexity and subject performance. J Neurosci. 31:14521–14530.

Palva JM, Zhigalov A, Hirvonen J, Korhonen O, Linkenkaer-Hansen K, Palva S. 2013. Neuronal long-range temporal correlations

and avalanche dynamics are correlated with behavioral scaling laws. Proc Natl Acad Sci USA. 110:3585–3590.
Pan WJ, Thompson GJ, Magnuson ME, Jaeger D, Keilholz S. 2013. Infraslow LFP correlates to resting-state fMRI bold signals. Neuroimage. 74:288–297.
Pereira J, Wang XJ. 2015. A tradeoff between accuracy and flexibility in a working memory circuit endowed with slow feedback mechanisms. Cereb Cortex. 25:3586–3601.
Perin R, Berger TK, Markram H. 2011. A synaptic organizing principle for cortical neuronal groups. Proc Natl Acad Sci USA. 108:5419–5424.
Plenz D, Thiagarajan TC. 2007. The organizing principles of neuronal avalanches: cell assemblies in the cortex? Trends Neurosci. 30:101–110.
Poulet JF, Petersen CC. 2008. Internal brain state regulates membrane potential synchrony in barrel cortex of behaving mice. Nature. 454:881–885.
Priesemann V, Wibral M, Valderrama M, Propper R, Le Van Quyen M, Geisel T, Triesch J, Nikoli D, Munk MH. 2014. Spike avalanches in vivo suggest a driven, slightly subcritical brain state. Front Syst Neurosci. 8:108.
Rajan K, Abbott LF. 2006. Eigenvalue spectra of random matrices for neural networks. Phys Rev Lett. 97:188104.
Ray S, Maunsell JH. 2011. Different origins of gamma rhythm and high-gamma activity in macaque visual cortex. PLoS Biol. 9:e1000610.
Rebert CS. 1973. Slow potential correlates of neuronal population responses in the cat's lateral geniculate nucleus. Electroencephalor Clin Neurophsyiol. 35:511–515.
Reimann MW, Anastassiou CA, Perin R, Hill SL, Markram H, Koch C. 2013. A biophysically detailed model of neocortical local field potentials predicts the critical role of active membrane currents. Neuron. 79:375–390.
Roberts JA, Boonstra TW, Breakspear M. 2015. The heavy tail of the human brain. Curr Opin Neurobiol. 31:164–172.
Rockstroh B, Elbert T, Canavan AGM, Lutzenberger W, Birbaumer N. 1989. Slow cortical potentials and behavior. Munich (Germany): Urban & Schwarzenberg.
Rubinov M, Sporns O, Thivierge JP, Breakspear M. 2011. Neurobiologically realistic determinants of self-organized criticality in networks of spiking neurons. PLoS Comput Biol. 7: e1002038.
Scholvinck ML, Maier A, Ye FQ, Duyn JH, Leopold DA. 2010. Neural basis of global resting-state fMRI activity. Proc Natl Acad Sci USA. 107:10238–10243.
Sethna JP. 2006. Statistical mechanics: entropy, order parameters, and complexity. New York: Oxford University Press.
Shew WL, Plenz D. 2013. The functional benefits of criticality in the cortex. Neuroscientist. 19:88–100.
Shriki O, Hansel D, Sompolinsky H. 2003. Rate models for conductance-based cortical neuronal networks. Neural Comput. 15:1809–1841.
Song S, Sjöström PJ, Reigl M, Nelson S, Chklovskii DB. 2005. Highly nonrandom features of synaptic connectivity in local cortical circuits. PLoS Biol. 3:e68.
Stanley HE. 1999. Scaling, universality, and renormalization: three pillars of modern critical phenomena. Rev Mod Phys. 71:S358–S366.
Tao T. 2011. Outliers in the spectrum of iid matrices with bounded rank perturbations. Probab Theory Rel. 155:231–263.
Truccolo W, Donoghue JA, Hochberg LR, Eskandar EN, Madsen JR, Anderson WS, Brown EN, Halgren E, Cash SS. 2011. Single-neuron dynamics in human focal epilepsy. Nat Neurosci. 14:635–641.
Turcotte DL. 1999. Self-organized criticality. Rep Prog Phys. 62:1377.
Vogels TP, Rajan K, Abbott LF. 2005. Neural network dynamics. Annu Rev Neurosci. 28:357–376.
von Stein A, Sarnthein J. 2000. Different frequencies for different scales of cortical integration: from local gamma to long range alpha/theta synchronization. Int J Psychophysiol. 38:301–313.
Wagenmakers EJ, Farrell S, Ratcliff R. 2004. Estimation and interpretation of $1/f^{\alpha}$ noise in human cognition. Psychon Bull Rev. 11:579–615.
Wang H, Stradtman GG, Wang XJ, Gao WJ. 2008. A specialized NMDA receptor function in layer 5 recurrent microcircuitry of the adult rat prefrontal cortex. Proc Natl Acad Sci USA. 105:16791–16796.
Wang XJ. 1998. Calcium coding and adaptive temporal computation in cortical pyramidal neurons. J Neurophysiol. 79: 1549–1566.
Wang XJ. 1999. Synaptic basis of cortical persistent activity: the importance of NMDA receptors to working memory. J Neurosci. 19:9587–9603.
Wang XJ. 2010. Neurophysiological and computational principles of cortical rhythms in cognition. Physiol Rev. 90:1195–1268.
Whittingstall K, Logothetis NK. 2009. Frequency-band coupling in surface EEG reflects spiking activity in monkey visual cortex. Neuron. 64:281–289.
Womelsdorf T, Valiante TA, Sahin NT, Miller KJ, Tiesinga P. 2014. Dynamic circuit motifs underlying rhythmic gain control, gating and integration. Nat Neurosci. 17:1031–1039.
Yoshimura Y, Dantzker JL, Callaway EM. 2005. Excitatory cortical neurons form fine-scale functional networks. Nature. 433:868–873.
Zhang Z, Seguela P. 2010. Metabotropic induction of persistent activity in layers II/III of anterior cingulate cortex. Cereb Cortex. 20:2948–2957.